HAL
open science

The water vapour distribution in the Arctic lowermost stratosphere during LAUTLOS campaign and related transport processes including stratosphere-troposphere exchange

A. Karpechko, A. Lukyanov, E. Kyrö, S. Khaikin, L. Korshunov, R. Kivi, H. Vömel

To cite this version:

A. Karpechko, A. Lukyanov, E. Kyrö, S. Khaikin, L. Korshunov, et al.. The water vapour distribution in the Arctic lowermost stratosphere during LAUTLOS campaign and related transport processes including stratosphere-troposphere exchange. Atmospheric Chemistry and Physics Discussions, 2006, 6 (3), pp.4727-4754. hal-00301530

HAL Id: hal-00301530

https://hal.science/hal-00301530v1

Submitted on 18 Jun 2008

HAL is a multi-disciplinary open access archive for the deposit and dissemination of scientific research documents, whether they are published or not. The documents may come from teaching and research institutions in France or abroad, or from public or private research centers.

L'archive ouverte pluridisciplinaire **HAL**, est destinée au dépôt et à la diffusion de documents scientifiques de niveau recherche, publiés ou non, émanant des établissements d'enseignement et de recherche français ou étrangers, des laboratoires publics ou privés.

Atmos. Chem. Phys. Discuss., 6, 4727–4754, 2006
www.atmos-chem-phys-discuss.net/6/4727/2006/
© Author(s) 2006. This work is licensed
under a Creative Commons License.

Atmospheric Chemistry and Physics Discussions

The water vapour distribution in the Arctic lowermost stratosphere during LAUTLOS campaign and related transport processes including stratosphere-troposphere exchange

A. Karpechko[1], A. Lukyanov[2], E. Kyrö[1], S. Khaikin[2], L. Korshunov[2], R. Kivi[1], and H. Vömel[3]

[1]Finnish Meteorological Institute, ARC, Sodankylä, Finland
[2]Central Aerological Observatory, Moscow, Russia
[3]Cooperative Institute for Environmental Sciences, University of Colorado, Boulder, USA

Received: 6 March 2006 – Accepted: 27 April 2006 – Published: 13 June 2006

Correspondence to: A. Karpechko (alex.karpetchko@fmi.fi)

Abstract

Balloon-borne water vapour measurements during January and February 2004, which were obtained as part of the LAUTLOS campaign at Sodankylä, Finland, 67° N, were used to analyse the water vapour distribution in the wintertime Arctic lowermost stratosphere. A 2.5 km thick layer (or 30 K in the potential temperature scale) above the local tropopause is characterized by a significant water vapour variability on a synoptic timescale with values between stratospheric and tropospheric, which is in good agreement with previously reported measurements. A cross-correlation analysis of ozone and water vapour confirms that this layer contains a mixture of stratospheric and tropospheric air masses. Some of the flights sampled laminae of enhanced water vapour above the tropopause. Meteorological analyses and backward trajectory calculations show that these features are related to filaments that had developed along the flanks of cut-off anticyclones, which had been active at this time over the Northern Atlantic. Cross-tropopause mass fluxes calculated following the Wei method are used to identify regions and processes that are important for stratosphere-troposphere exchange (STE) in high-latitudes. Intensive STE occurs around cut-off anticyclones in regions of strong winds, where calculations suggest the presence of developed clear-air turbulence. The decay of the filaments is also shown to be important for STE.

1 Introduction

Water vapour is a very important gas for the radiative state of the upper troposphere-lower stratosphere (UTLS) region. Calculations by Forster and Shine (2002) indicate that water vapour trends reported by Oltmans et al. (2000) may have resulted in a cooling of the lower stratosphere of 0.8 K over two decades. Water vapour is also crucial for the chemical balance of the UTLS region through its role as a source of the hydroxyl radical (Esler et al., 2001), which is the main oxidant in the atmosphere. Therefore, a correct prediction of future climate requires a detailed knowledge of the

water vapour distribution in the UTLS as well as the mechanisms regulating it.

Air enters the stratosphere mainly in the tropics and, therefore, processes at the tropical tropopause are of primary importance for our understanding of the water vapour distribution in the entire stratosphere. However, in the extratropics water vapour in the first few kilometres above the tropopause is largely controlled by extratropical troposphere-to-stratosphere transport (TST) (Dessler et al., 1995; Hintsa et al., 1998). This transport is either quasi-isentropic in the vicinity of the jet streams (Hoerling et al., 1993), or diabatic inside of convection (Poulida et al., 1996). As a result, a mixing layer consisting of stratospheric and tropospheric air forms above the tropopause (Ray et al., 1999, Fisher et al., 2000). Satellite measurements of water vapour provide a global picture of its distribution in the lowermost stratosphere and are able to describe seasonal and interannual variations (see Chiou et al., 1997; Pan et al., 1997; Randel et al., 2001; Nedoluha et al., 2002; Randel et al., 2004, and references therein). However, since satellites have a limited spatial resolution, detailed process studies in the UTLS region can be based on in situ measurements only.

Several water vapour in situ campaigns have been performed in the Arctic (Kelly et al., 1990; Ovarlez, 1991; Ovarlez and Ovarlez, 1994; Vömel et al., 1997), but only few have concentrated on the processes in the Arctic lowermost stratosphere. Murphy et al. (1990) detected ice saturation at the winter Arctic tropopause in ER-2 aircraft observations. Pfister et al. (2003) used aircraft measurements during the SOLVE campaign 1999/2000 and estimated the vertical extent of the water vapour TST transport in the Arctic. Krebsbach et al. (2006) analysed the seasonality and variability of water vapour in the lowermost stratosphere within the broad latitude belt of 30° N to 80° N using aircraft measurements from the SPURT project. However, detailed studies of the transport events that contribute to the formation of the tropopause mixing layer in the Arctic have not yet been published.

This paper presents balloon borne water vapour measurements obtained during the LAPBIAT Upper Troposphere Lower Stratosphere (LAUTLOS) project. The campaign took place from 29 January 2004 to 27 February 2004 at Sodankylä, Finland, 67.4° N,

26.6° E, and was aimed at the intercomparison of lightweight balloon borne instruments (Suortti et al., 2006[1]). It provided 11 high-accuracy water vapour profiles within a period of one month. This data set provides a suitable statistics to study the water vapour variability on synoptic time scales. Results related to polar vortex dynamics are discussed in Maturilli et al. (2006). This present study concentrates on the tropopause region and its main purpose is to present a detailed case study of transport processes contributing to the formation of a mixing layer above the tropopause in the winter Arctic. Attention is given to filamentation around upper level cut-off anticyclones since this process was linked to layers of enhanced water vapour in the lowermost stratosphere observed in several profiles during the campaign. The paper starts with a description of the data set and the tools used in this study. The distribution of water vapour in the lowermost stratosphere during the campaign is analysed in different vertical coordinates. Case studies demonstrate the effects of transport associated with filamentation of upper-level cut-off anticyclones on the water vapour distribution. The relative importance of the different processes for stratosphere-troposphere exchange (STE) in high-latitudes is estimated by calculating cross-tropopause fluxes.

2 Data sets and tools

The main goal of LAUTLOS was the intercomparison of different types of hygrometers. For this purpose, several water vapour instruments were launched onboard the same balloon payload. The NOAA/CMDL frost point hygrometer, which has the longest record of stratospheric water vapour observation at Boulder, CO (Oltmans et al., 2000), was used as reference instrument. This instrument uses two different sensitivity regimes: a lower setting, which allows the instrument to measure tropospheric

[1]Suortti, T. M., Miloshevich, L. M., Paukkunen, A., Leiterer, U., Kivi, R., Vömel, H., Yushkov, V., Ruppert, P., Neuber, R., and Kämpher, N.: The LAUTLOS-WAVAP: Tropospheric comparisons, J. Atmos. Oceanic Technol., submitted, 2006.

water vapour, and a higher setting, better suited for stratospheric measurements. During LAUTLOS, the sensitivity change typically occurred in the lowermost stratosphere causing some data loss in this region (Vömel et al., 2006[2]). Here, we use water vapour measurements obtained by the FLASH-B instrument (Yushkov et al., 1998; Yushkov et al., 2000), which provided the largest number of successful water vapour profiles in the lowermost stratosphere. The NOAA/CMDL frost point hygrometer and the FLASH-B instrument show excellent agreement between 15 and 25 km (Vömel et al., 2006[2]) and the results are therefore independent of the choice of instrument.

The FLASH-B hygrometer is based on the fluorescent method. It uses the photodissosiation of the H_2O molecules that are exposed to vacuum ultraviolet radiation at a wavelength of 121.6 nm (Lyman-alpha hydrogen emission). The exited OH radical fluoresces in the range of 306–314 nm and the fluorescence is detected by a photomultiplier operated in photon counting mode. For stratospheric conditions the intensity of the fluorescent light is proportional to the water vapour mixing ratio. The estimated measurement uncertainty does not exceed 10%. Altogether, 11 water vapour profiles have been obtained by FLASH-B between 29 January 2004 and 27 February 2004. Only descent data, which avoid balloon contamination, are used here.

Ozone was measured using ECC ozonesondes connected to the NOAA/CMDL frost point hygrometer flying on the same payload as FLASH-B. The ECC sensor is significantly slower than FLASH-B and to correct for this sensor delay, the ozone signal in all profiles was advanced by 30 s as part of the analysis. This time lag corresponds to a sensor response time at a sensing solution temperature of about 278 K (Bethan et al., 1996). However, the effect of the relatively long response time is not only to delay signal, but also to integrate it in space. This might be taken into account in the interpretation of the results that rely on the simultaneity of water vapour and ozone measurements, although the effect is not expected to be significant.

[2]Vömel, H., Yushkov, V., Khaykin, S., Korshunov, L., Kyrö, E., and Kivi, R.: Intercomparisons of stratospheric water vapor sensors: FLASH-B and NOAA/CMDL frost point hygrometer, J. Atmos. Oceanic Technol., in review, 2006.

For back-trajectories and cross-tropopause flux estimations the trajectory model described by Lukyanov et al. (2003) is used. Meteorological analyses and forecast data are from the operational ECMWF T511L60 model.

3 Observations

The distribution of water vapour in the tropopause region during the LAUTLOS campaign is shown in Fig. 1 as a function of different vertical coordinates. Figure 1a shows the water vapour mixing ratio (WVMR) as a function of potential temperature (θ). Studying potential temperature is not very useful for water vapour transport between the troposphere and the stratosphere, since it gives no information about the location of the tropopause. However, it is a natural way to put the data into context of the general circulation as well as to provide a suitable reference for comparison with other water vapour measurements. This figure shows that the highest level where noticeable flight-to-flight variability is observed is about 345 K. Up to this level, WVMR exceeds, at times significantly, 6–7 ppmv, suggesting that air contains a significant fraction of tropospheric origin, i.e. air that has not passed through the tropical "cold trap" tropopause. Between 345 K and 360–380 K, WVMR shows values of about 4 ppmv with little flight-to-flight variability. Such low water vapour values suggest that the direct tropospheric contribution is not significant, though a small fraction of tropospheric origin might still be found at these levels. WVMR averaged over all flights is 4.1 ppmv at 350 K, whereas a minimum of 3.9 ppmv is observed at 365 K. Given the overall downward transport in the wintertime extratropical stratosphere, the small WVMR increase between 365 K and 350 K might be attributed to mixing across the extratropical tropopause.

Estimates of the upper limit for penetration of tropospheric air found in the literature are close to our results. Measurements of reactive organic species (Scheeren et al., 2003) indicate that the fraction of tropospheric air in the mid latitude lowermost stratosphere during March 1997 approached zero at about 350 K. Similar results were obtained by Chen (1995), who found very little TST in winter above 340 K using semi-

Lagrangian transport model simulations.

More suitable for studies of STE are vertical coordinates that are centred at the tropopause. Figure 1b shows water vapour as a function of height above the lapse rate tropopause (WMO definition). The flight-to-flight variability nearly disappears 2.5 km above the tropopause. This is slightly higher than the value of 1.8 km obtained from Arctic aircraft measurements in mid-winter 2000 (Pfister et al., 2003). Typical stratospheric WVMR values of less than 5 ppmv are reached already at 1–1.7 km above the tropopause in 9 out of 11 profiles, while only two flights sampled enhanced WVMR higher than two kilometres above the tropopause. In all profiles WVMR continues to decrease with altitude up to the WVMR minimum, which is reached between 2.75 and 5 km above the tropopause. The average over all soundings shows a minimum of 3.9 ppmv at 3 km above the tropopause.

Hoor et al. (2004) have shown that the CO distribution in the lowermost stratosphere correlates very well with the distance from the local dynamical tropopause expressed in the potential temperature ($\Delta\theta_d$) and the scatter is significantly reduced compared to θ coordinate. Krebsbach et al. (2006) found a good correlation between $\Delta\theta_d$ and H_2O and O_3. Here, $\Delta\theta$ is calculated with respect to both the thermal ($\Delta\theta_t$) and the dynamical ($\Delta\theta_d$) tropopause. The distribution of the LAUTLOS water vapour measurements in $\Delta\theta_t$ coordinates calculated with respect to the local thermal tropopause is shown in Fig. 1c. The flight-to-flight variability almost disappears at $\Delta\theta_t$=30 K, except for one profile which shows enhanced WVMR as high as $\Delta\theta_t$=40 K above the local tropopause. However, comparing Fig. 1c and a shows that the scatter of the data is not reduced by the introduction of the $\Delta\theta_t$ coordinate and it is not evident that the water vapour distribution follows the shape of the thermal tropopause rather than the isentropic surfaces. Figure 1d shows the water vapour distribution in $\Delta\theta_d$ coordinates calculated with respect to the dynamical tropopause which is obtained from the ECMWF potential vorticity (PV) and potential temperature fields. To find θ at the dynamical tropopause, the vertical profiles of PV and θ were first constructed at the locations where the balloons crossed the thermal tropopause during descent. Then, θ was interpolated to the

level of PV=3.5 PVU. Linear interpolation between model grid points was used both in horizontal and vertical. A value of 3.5 PVU was chosen because it corresponds well to the thermal tropopause in the extratropics (Hoelring et al., 1993). Using the $\Delta\theta_d$ coordinate noticeably reduces the WVMR scatter above the tropopause compared to Fig. 1a through c, with values gradually decreasing with height until stratospheric values are reached at about $\Delta\theta_d$=30 K. This is slightly higher than value of 25 K found by Hoor et al. (2004) in CO observations.

Plotting water vapour against a tracer of stratospheric air is another possibility to assess mixing of stratospheric and tropospheric air. Figure 2 shows water vapour plotted against ozone. Note that only data from 9 flights are presented here, since ozone observations were not available on 15 February 2004 and 25 February 2004. While stratospheric air is characterized by high ozone and low water vapour, tropospheric air is characterized by high water vapour and low ozone. Mixing lines with intermediate values of ozone and water vapour are evident in Fig. 2 and can be formed only by irreversible mixing of tropospheric and stratospheric air (e.g. Hoor et al., 2002). The spread of water vapour values decreases noticeably between ozone values of 200 and 300 ppbv, and there is almost no variability above 400 ppbv. This is in agreement with values of 300–500 ppbv noted by Pfister et al. (2003) as an upper limit for the penetration of the tropospheric air into the stratosphere. To determine the depth of the mixing layer, the data in Fig. 2 are colour-coded according to θ. The mixing region extends up to 340–345 K, which is close to the upper level of the flight-to-flight variability shown in Fig. 1a and is slightly higher than the value of 330 K found in aircraft observations of O_3 and CO (Hoor et al., 2002). This difference may be related to the different tracers or the different measurement technique that was used. Interannual variability in tropopause dynamics cannot be excluded either.

In the tropopause region, a laminated structure in the vertical profiles of trace gases that have a strong gradient across the tropopause is usually indicative of recent transport. These cases are of particular interest in our study. Figure 3a shows the profiles of water vapour and ozone obtained on 17 February 2004. Here, the pronounced WVMR

maximum and the corresponding ozone minimum are centred at 330 K, well above the local tropopause. This suggests recent transport of air with a large tropospheric fraction that has not yet been mixed with its surroundings. A similar event, but less pronounced and centred at 340 K, was observed on 24 February 2004 (Fig. 3b). To investigate these events more thoroughly, the meteorological situation of the tropopause region is analysed and discussed in the next session.

4 Meteorological situation

The measurement period (late January to late February 2004), was characterised by high anticyclonic activity over the Northern Atlantic, which was linked to a low phase of the Northern Atlantic Oscillation (NAO) index. The upper troposphere over Northern Scandinavia was mostly dominated by a long wave trough. Accordingly, the average tropopause pressure at Sodankylä was a higher than normal. Note that a low tropopause in the Arctic is one of the known characteristics of a low NAO index (Ambaum and Hoskins, 2002). Only for a short period (18 February–20 February 2004), the station was located on the anticyclonic side of the jet stream and the tropopause rose up to 12.5 km (166 hPa).

During February, several cut-off anticyclones developed over the eastern part of the Northern Atlantic following amplifications of the upper-level quasi-stationary ridge. One such cut-off anticyclone (hereafter A1) formed on 14 February 2004 just north of the British Isles. The development of the meteorological situation at the tropopause level can be seen in Fig. 4 which shows 330 K isentropic maps of water vapour obtained from ECMWF data.

The use of water vapour as a tracer for synoptic-scale transport in the UTLS has been utilized in a number of studies (Appenzeller and Davies, 1992; Gray et al., 1994; Beuermann et al., 2002). The water vapour distribution is able to reproduce large-scale systems, which appear on more traditional PV maps, and gives a more detailed picture of processes on smaller scales. Differences between tracer properties of wa-

ter vapour and PV were discussed by Simmons et al. (1999). First, PV, unlike water vapour, is subject to non advective processes like radiation. Second, water vapour in the ECMWF model is defined directly on the model grid, whereas PV is derived from dynamical fields represented spectrally. For these reasons, Simmons et al. (1999) suggested that water vapour provides a record of earlier synoptic events than PV does. It can be added that the vertical gradients of water vapour in the vertical range of interest is stronger than that of PV. Therefore, water vapour shows stronger gradients on isentropic surfaces due to differential advection.

Figures 4 show that an area of higher water vapour (and lower PV) associated with A1 was advected southeastwardly for several days, before it finally dissipated over the Eastern Mediterranean. Note that the centre of A1 is drier than its flanks. This may be explained by saturation and subsequent dehydration that occurred around 12 February 2004 when temperatures at the 330 K isentropic level in the centre of the developing anticyclone were as cold as 200 K (saturation mixing ratio of about 7 ppmv). In the early stage of the development of A1, an area of enhanced water vapour became elongated meridionally north of A1 (Fig. 4b–d) and by 16 February 2004 a thin water vapour filament had formed. On 16 February 2004, 18:00 UTC this filament was located above Sodankylä (Fig. 4e). The sounding on 16 February 2004, 18:00 UTC sampled enhanced water vapour up to 335 K with a small local maximum of WVMR around 345 K. At 325 K, 16 ppmv of water vapour were measured, which was the highest WVMR value at this level for the entire campaign. Growing wavelike perturbations along the filament finally led to its break up. However, remnants still appeared in the vicinity of the station on 17 February 2004, 18:00 UTC (Fig. 4g) when a layer of enhanced water vapour and reduced ozone mixing ratios was observed (Fig. 3a). During 16–17 February 2004, while the filament was located above the station, Northern Scandinavia was influenced by an upper-level trough and the tropopause in Sodankylä was located at 310 K. To clearly identify the origin of this moist air, back trajectories were run starting 16 February 2004, 18:00 UTC and 17 February 2004, 18:00 UTC at 330 K clustered around the station. As shown in Fig. 4, these trajectories followed the humid filament

and on 14 February 2004 were located over the Northern Atlantic on the western flank of A1. Note that there is no indication that these trajectories crossed the tropopause (shown as a region between the 2 and 3.5 PVU contours) after 14 February 2004. This suggests that the humid layer sampled on 17 February 2004 at 330 K was generated by transport from the lower levels of the mixing layer to which moisture must have been supplied from the troposphere in earlier events.

Analyses of water vapour isentropic maps reveal that the development of filaments similar to the one described above often accompany the development of cut-off anticyclones over the Northern Atlantic during January–February 2004. Figure 4h captures another filament on 18 February 2004, 18:00 UTC that stretched meridionally along approximately 30° E, northeast of the area of low PV located over the Greenland Sea. The corresponding anticyclone (hereafter A2) became cut-off over the Northern Atlantic on 17 February 2004 and was more intensive and stationary than A1. As A2 approached the station, a balloon sounding on 18 February 2004, 18:00 UTC sampled a high tropopause at 320 K and enhanced values of WVMR up to 345 K.

An example of a humid filament at 340 K is shown in Fig. 5. The filament is curved above the Baltic Sea and Finland and stretched rather zonally between 15° E and 60° E. The passage of this filament near Sodankylä on 24 February 2004, 18:00 UTC corresponded to the detection of the layer of enhanced water vapour and reduced ozone shown in Fig. 3b. Backward trajectories starting on this day suggest a very different situation. This air mass was involved in filamentation on 18 February 2004 during a poleward Rossby wave breaking event over the Aleutian Sea (not shown) and was subsequently advected for 6 days across North America and the Atlantic Ocean before being probed at Sodankylä.

The development of cut-off anticyclones, which from the dynamical point of view can be regarded as poleward Rossby-wave breaking, usually occurs in regions of diffluence over the eastern Atlantic and eastern Pacific. Contour advection simulations of these events revealed a structure richer than available in operational analyses at that time (Peters and Waugh, 1996), including the development of fine scale filaments similar

to those shown here in the water vapour fields. Therefore, our case study analysis is useful even from a climatological perspective. Strong distortion of the tropopause associated with Rossby-wave breaking, both poleward and equatorward, is usually followed by non conservative processes such as diabatic heating and cooling or turbulent mixing (Holton et al., 1995). Low PV anomalies merge with the tropospheric jet a few days after their development and a large part of the tropospheric air contained in the cut-off anticyclones usually returns back to the troposphere. However, our observations demonstrate that processes during the lifecycle of cut-off anticyclones can lead to a noticeable distortion of the chemical composition in the lowermost stratosphere at high latitudes. A remaining question is: how important are these processes for mixing of stratospheric and tropospheric air and, hence, for the formation of the mixing layer above the tropopause? To describe this mixing more quantitatively, we calculated cross-tropopause fluxes, which are described and analysed in the next section.

5 Cross-tropopause flux associated with cut-off anticyclones

There are several studies of STE in the extratropics (Hoelring et al., 1993; Siegmund et al., 1996; Wirth and Egger, 1999; Kowol-Santen et al., 2000; Sigmond et al., 2000; Wernli and Bourqui, 2002), which are based on analyzed winds and focused on the estimation of local instantaneous cross-tropopause flux (CTF). These studies applied both Eulerian methods based on Wei's formula (Wei, 1987) and Lagrangian methods based on trajectory calculations. Siegmund et al. (1996) found that for accurate estimates of the local and instantaneous CTF, the spatial and temporal resolution of the analyzed data should be at least $1^\circ \times 1^\circ$ and 6 h, respectively. In the present study, the transport of air through the tropopause over the Northern Atlantic and Europe during LAUTLOS is investigated using a trajectory model and analyzed winds from the T511 ECMWF model (horizontal resolution $0.5^\circ \times 0.5^\circ$ and temporal resolution 6 h). The method used here is based on the formula by Wei with PV as a vertical coordinate. The

CTF is defined as:

$$F = -\frac{1}{g}\frac{\partial p}{\partial PV}\frac{dPV}{dt}, \quad (1)$$

where p is the pressure and g is the acceleration due to gravity. The unit of F is kg m^{-2} s^{-1}. Following Sigmond et al. (2000) the material derivative of PV is estimated using a Lagrangian approach. 6 h forward and backward trajectories are initiated at each grid point and PV values at the end points of trajectories are used for the estimation of the PV tendency. The partial derivative $\frac{\partial p}{\partial PV}$ is calculated on each grid point by using pressure values on PV levels adjacent to the tropopause. Due to the combination of calculations on the grid and along the trajectories this method can be considered as "semi-Lagrangian". Fluxes are calculated through the 3.5 PVU isosurface of PV used to define the dynamical tropopause. We concentrate our analysis on the period from 14 to 19 February 2004, which largely covers the lifetime of A1. Examples of fluxes for selected dates are shown in Fig. 6.

Two primary physical processes are responsible for changes in PV (and therefore for CTF), i.e. small-scale turbulence and diabatic heating. In anticyclones, clear-air turbulence (CAT) can form in the region of strong winds surrounding the anticyclone. Diabatic heating in anticyclones is associated with temperature anomalies, which was studied in the axisymmetric balanced model by Zierl and Wirth (1997). It is expected to be stronger in the centre of the anticyclone where the temperature anomaly is larger. This process leads to a one-way mass transfer from the troposphere to the stratosphere.

Analyses show that the strongest fluxes (upward and downward) are concentrated in the tropopause-slope region, i.e. along the potential temperature contours in Fig. 6. Note that the concentration of potential temperature contours also marks regions of strong winds. On 14 February 2004, 18:00 UTC (Fig. 6a), the jet stream bends around A1 centred east of Iceland. On 15 February 2004 (Fig. 6c), the jet stream moves with A1 towards Scandinavia, weakening at the same time. By 17 February 2004, when A2 starts forming over the Northern Atlantic, the jet stream intensifies northeast of the

Greenland (Fig. 6e). Calculations of the CAT index (see Traub and Lelieveld, 2003) show that the strongest fluxes often coincide with areas of strong turbulence near the jet stream (Fig. 6b, d, f). This subjective conclusion is supported by the correlation between the area-integrated CTF and the CAT index. Figure 7 shows a time series of the area-integrated upward and downward CTF together with the CAT index for the whole period calculated in 6-h time steps. All quantities are integrated over the area between 310° W and 60° E longitudes and between 60° N and 85° N latitudes. It is seen that the minimum of the area-averaged CAT index around 16 February 2004 corresponds to a minima in both upward and downward fluxes. The increase of the CAT index after 18 February 2004, associated with the intensification of the jet stream around A2, coincides with an increase in both fluxes. Absolute values of the correlation coefficient between the CAT index and the upward and downward fluxes are 0.69 and 0.75 respectively. These results suggest that the turbulence at the flanks of cut-off anticyclones is important for the mixing across the tropopause. At the same time the CTF in the central part of anticyclones is much weaker (see Fig. 6), suggesting that diabatic heating associated with cut-off anticyclones is of less importance.

Significant fluxes are found also away from the jet stream (Fig. 6), where the CAT index according to our calculations is significantly weaker. An example is given in Fig. 6e for 17 February 2004, 12:00 UTC. Strong fluxes of both signs appear along the jet stream that was stretched meridionally at approximately 320° W up to 80° N and across the Norwegian Sea towards the south-western tip of the Scandinavia. Besides these examples, areas of strong upward fluxes are seen adjacent to remnants of the filament (i.e. areas of higher potential temperature) south of Spitsbergen and north of Greenland. A noticeable decrease in filament size, which is observed at the same time, suggests that these fluxes are associated with the decay of the filament. Figure 6a shows fluxes associated with another filament that was stretched meridionally at approximately 45° E west of the Franz Josef Land islands. Downward fluxes are seen adjacent to the filaments north of Greenland in Fig. 6a and north of Spitsbergen in Fig. 6b. Based on our calculations, it is not possible to deduce unambiguously the

cause of these fluxes. An influence of turbulence cannot be excluded based only on CAT index calculations. Also radiative decay could play a significant role. However, in the case of a warm filament, the radiative decay would result in upward fluxes whereas the calculations reveal fluxes of both signs. The disappearance of filaments may also be attributed to a truncation effect, i.e. a filament becomes too thin to be resolved by the analysis.

Attention should also be given to the fact that the operational analyses used for the CTF calculations are not dynamically consistent. This can introduce spurious mixing, which was pointed out by Stohl et al. (2004). To quantify the influence of these inconsistencies on our estimations, we repeated the CTF calculations for the same period using ECMWF forecast fields. The forecasts were initiated on 13 February 2004, 12:00 UTC. The spatial structure of the forecasted CTF fields is similar to that of the analysed fields with largest fluxes concentrated along the tropopause-slope regions. Area-integrated upward and downward fluxes are shown in Fig. 7 together with those calculated from the analyses. It is seen that the forecasted fluxes are weaker than the analysed ones. In average, the difference is 23% for the upward fluxes and 17% for the downward fluxes. However, their temporal behaviours are quite similar. The forecasted fluxes also show a minimum around 16 February 2004 and an increase after 18 February 2004. Absolute values of the correlation coefficient between the CAT index and upward and downward fluxes calculated from the forecasted fields are 0.52 and 0.95 correspondingly. Therefore, the use of analysed instead of forecasted fields influences our results quantitatively rather than qualitatively.

The fluxes shown in Fig. 7 have been integrated over the whole domain including areas not coloured in Fig. 6, where absolute values of the fluxes are small (less than 3×10^{-2} kg m^{-2} s^{-1}). It is therefore necessary to comment on the contribution and significance of these "weak" fluxes. During the study period 'weak' fluxes contribute on average 29% and 36% to the analysed upward and downward fluxes integrated over the whole domain and do not reveal any noticeable response to changes in the meteorological situation. Though one can argue that this is a significant contribution to

the quantitative estimations shown in Fig. 7, our conclusions concerning the regions of a prime importance for the STE remain nevertheless valid. A part of the "weak" fluxes can be attributed to numerical noise; however, there is no clear way how to choose a threshold for a separation between real transport and noise (see Gettelman and Sober, 2000).

6 Conclusions

Balloon-borne water vapour measurements obtained during the LAUTLOS campaign in January–February 2004 at Sodankylä, Finland, 67° N were used to analyse the water vapour distribution in the wintertime Arctic lowermost stratosphere and to identify mechanisms that are important for the formation of the observed distribution. A significant variability of water vapour due to synoptic processes at the tropopause was observed up to 345 K with much smaller variability in the upper part of the lowermost stratosphere (up to the stratospheric polar vortex). The layer above the tropopause that is significantly influenced by transport through the extratropical tropopause is approximately 2.5 km (or 30 K in the potential temperature) thick and follows the shape of the dynamical rather than the thermal tropopause. Cross-correlation analyses of ozone and water vapour confirm that this layer contains a mixture of stratospheric and tropospheric air. Water vapour concentrations continue to decrease up to about 365 K (3–5 km above the local tropopause), the level of the hygropause, and an influence of the extratropical troposphere up to the hygropause cannot be excluded. Indeed, there are observational evidences for transport of tropospheric ozone up to 360–380 K in winter (Vaughan and Timmis, 1998).

The distribution of water vapour up to 345 K was strongly influenced by transport processes associated with cut-off anticyclones which were active during the campaign over the Northern Atlantic. Calculations of the CTF over the Northern Atlantic and Europe show that two-way STE occurs mainly in the tropopause-slope regions i.e. regions where isentropic surfaces cross the dynamical tropopause. The strongest CTF was ob-

served around cut-off anticyclones and is attributed to clear air turbulence, which forms in the region of strong winds surrounding anticyclones. This conclusion is in line with Traub and Lelieveld (2003), who have found a connection between the upward flux and the CAT index, associated with the monsoon circulation over the eastern Mediterranean in summer. Significant CTF is also observed along filaments that developed at the flanks of cut-off anticyclones. These filaments quite often accompanied a development of cut-off anticyclones during late winter 2004, and were sampled by balloons as layers of enhanced water vapour and reduced ozone. Based on our results, filamentation associated with cut-off anticyclones can significantly contribute to TST of water vapour in the Northern Atlantic and European region.

Acknowledgements. The LAUTLOS campaign was funded by the EU under projects LAPBIAT and Cost 723. We thank the entire LAUTLOS team for their excellent work. A. Karpechko, E. Kyrö, and R. Kivi acknowledge support from the Finnish Academy under project FARPOCC. A. Lukyanov, S. Khaikin, and L. Korshunov acknowledge support from the International Science & Technology Center (ISTC) under projects #3093 and #3095. We would like to thank ECMWF for providing meteorological data. Calculations of PV and interpolations of the data on the isentropic levels were done using codes developed by H. Wernli.

References

Ambaum, M. H. and Hoskins, B. J.: The NAO troposphere-stratosphere connection, J. Climate, 15, 1969–1978, 2002.

Appenzeller, C. and Davies, H. C.: Structure of stratospheric intrusions into the troposphere, Nature, 358, 570–572, 1992.

Bethan, S., Vaughan, G., and Reid, S. J.: A comparison of ozone and thermal tropopause heights and the impact of tropopause definition on quantifying the ozone content of the tropopause, Q. J. R. Meteorol. Soc., 122, 929–944, 1996.

Beuermann, J., Konopka, P., Brunner, D., Bujok, O., Günther, O., McKenna, D. S., Lelieveld, J., Muller, R., and Schiller, C.: High-resolution measurements and simulation of stratospheric and tropospheric intrusions in the vicinity of the polar jet stream, Geophys. Res. Lett., 29, doi:10.29/2001GL014162, 2002.

Chen, P.: Isentropic cross-tropopause mass exchange in the extratropics, J. Geophys. Res., 100(D8), 16 661–16 673, 1995.
Chiou, E. W., McCormick, M. P., and Chu, W. P.: Global water vapor distribution in the stratosphere and upper troposphere derived from 5.5 years of SAGE II observations (1986–1991), J. Geophys. Res., 102(D15) 19 105–19 118, 1997.
Dessler, A. E., Hintsa, E. J., Weinstock, E. M., Anderson, J. G., and Chan, K. R.: Mechanisms controlling water vapour in the lower stratosphere: A tale of two stratospheres, J. Geophys. Res., 100(D11), 23 167–23 172, 1995.
Esler, J. G., Tan, D. G. H., Haynes, P. H., Evans, M. J., Law, K. S., Plantevin, P.-H., and Pyle, J. A.: Stratosphere-troposphere exchange: Chemical sensitivity to mixing, J. Geophys. Res., 106(D5), 4717–4731, 2001.
Fisher, H., Wienhold, F.-G., Hoor, P., Bujock, O., Schiller, C., Siegmund, P., Ambaum, M., Scheeren, H. A., and Lelieveld, J.: Tracer correlations in the northern high latitude lowermost stratosphere: Influence of cross-tropopause mass exchange, Geophys. Res. Lett., 27, 97–100, 2000.
Forster, P. M. de F. and Shine, K. P.: Assessing the climate impact of trends in stratospheric water vapor, Geophys. Res. Lett., 29(6), 1086, doi:10.1029/2001GL01390, 2002.
Gettelman, A. and Sobel, A. H.: Direct diagnoses of stratosphere-troposphere exchange, J. Atmos. Sci., 57, 3–16, 2000.
Gray, L. J., Bithell, M., and Cox, B. D.: The role of specific-humidity fields in the diagnosis of stratosphere troposphere exchange, Geophys. Res. Lett., 21, 2103–2106, 1994.
Hintsa, E. J., Boerling, K. A., Weinstock, E. M., Anderson, J. G., Gary, B. L., Pfister, L., Daube, B. C., Wofsy, S. C., Loewenstein, M., Podolske, J. R., Margitan, J. J., and Bui, T. P.: Troposphere-to-stratosphere transport in the lowermost stratosphere from measurements of H_2O, CO_2, N_2O, and O_3, Geophys. Res. Lett., 25, 2655–2658, 1998.
Hoerling, M. P., Schaack, T. K., and Lenzen, A. J.: A global analysis of Stratospheric-tropospheric exchange during Northern Winter, Mon. Wea. Rev., 121, 162–172, 1993.
Holton, J., Haynes, P., McIntyre, M., Douglass, A., Rood, R., and Pfister, L.: Stratosphere-troposphere exchange, Rev. Geophys., 33, 403–440, 1995.
Hoor, P., Fischer, H., Lange, L., Lelieveld, J., and Brunner, D.: Seasonal variations of a mixing layer in the lowermost stratosphere as identified by the CO-O3 correlation from in situ measurements, J. Geophys. Res., 107, 4044, doi:10.1029/2000JD000289, 2002.
Hoor, P., Gurk, C., Brunner, D., Hegglin, M. I., Wernli, H., and Fischer, H.: Seasonality and

extent of extratropical TST derived from in-situ CO measurements during SPURT, Atmos. Chem. Phys., 4, 1427–1442, 2004.
Kelly, K. K., Tuck, A. F, Heidt, L. E., Loewenstein, M., Podolske, J. R., Strahan, S. E., and Vedder, J. F.: A comparison of ER-2 measurements of stratospheric water vapour between the 1987 Antarctic and 1989 Arctic airborne missions, Geophys. Res. Lett., 17(4), 465–468, 1990.
Kowol-Santen, J., Elbern, H., and Ebel, A.: Estimation of cross-tropopause airmass fluxes at midlatitudes: Comparison of different numerical methods and meteorological situations, Mon. Wea. Rev., 128, 4045–4057, 2000.
Krebsbach, M., Schiller, C., Brunner, D., Günther, G., Hegglin, M. I., Mottaghy, D., Riese, M., Spelten, N., and Wernli, H.: Seasonal cycles and variability of O3 and H2O in the UT/LMS during SPURT, Atmos. Chem. Phys., 6, 109–125, 2006.
Lukyanov, A., Nakane, H., and Yushkov, V.: Lagrangian estimations of ozone loss in the core and edge region of the arctic polar vortex 1995/1996: Model results and observations, J. Atmos. Chem., 44(2), 191–210, 2003.
Maturilli, M., Fierli, F., Yushkov, V., Lukyanov, A., Khaykin, S., and Hauchecorne, A.: Stratospheric Water Vapour in the Vicinity of the Arctic Polar Vortex, Ann. Geophys., in print, 2006.
Murphy, D. M., Kelly, K. K., Tuck, A. F., and Proffitt, M. H.: Ice saturation at the tropopause observed from ER-2 aircraft, Geophys. Res. Lett., 17, 353–356, 1990.
Nedoluha, G. E., Bevilacqua, R. M., Hoppel, K. W., Lumpe, J. D., and Smit, H.: Polar Ozone and Aerosol Measurement III measurements of water vapor in the upper troposphere and lowermost stratosphere, J. Geophys. Res., 107(D10), 4103, doi:10.1029/2001JD000793, 2002.
Oltmans, S. J., Vömel, H., Hofmann, D. J., Rosenlof, K. H., and Kley, D.: The increase in stratospheric water vapor from balloonborne frost-point hygrometer measurements at Washington, D.C., and Boulder, Colorado, Geophys. Res. Lett., 21, 3453–3456, 2000.
Ovarlez, J.: Stratospheric water vapor measurements during CHEOPS-3, Geophys. Res. Lett., 18(4), 771–774, 1991.
Ovarlez, J. and Ovarlez, H.: Stratospheric water vapor content evolution during EASOE, Geophys. Res. Lett., 21(13), 1235–1238, 1994.
Pan, L., Solomon, S., Randel, W., Lamarque, J. F., Hess, P., Gille, J., Chiou, E. W., and McCormick, M. P.: Hemispheric asymmetries and seasonal variations of the lowermost stratospheric water vapour and ozone derived from SAGE II data, J. Geophys. Res., 102(D23),

28 177–28 184, 1997.
Peters, D. and Waugh, D. W.: Influence of barotropic shear on the poleward advection of upper-tropospheric air, J. Atmos. Sci., 53, 3031–3013, 1996.
Pfister L., Selkirk, H. B., Jensen, E. J., Podolske, J., Sachse, G., Avery, M., Schoeberl, M. R., Mahoney, M. J., and Richard, E.: Processes controlling water vapor in the winter Arctic tropopause region, J. Geophys. Res., 108(D5), 8314, doi:10.1029/2001JD001067, 2003.
Poulida, O., Dickerson, R. P., and Heymsfield, A.: Stratosphere-troposphere exchange in a midlatitude mesoscale convective complex 1 observations, J. Geophys. Res., 101, 6823–6836, 1996.
Randel, W. J., Wu, F., Gettelman, A., Russell III, J. M., Zawodny, J. M., and Oltmans, J.: Seasonal variation of water vapor in the lower stratosphere observed in Halogen Occultation Experiment data, J. Geophys. Res., 106(D13), 14 313–14 326, 2001.
Randel, W. J., Wu, F., Oltmans, S. J., Rosenlof, K., and Nedoluha, G.: Interannual changes of stratospheric water vapor and correlations with tropical tropopause temperatures, J. Atmos. Sci., 61, 2133–2148, 2004.
Ray, E. A., Moore, F. L., Elkins, J. W., Dutton, G. S., Fahey, D. W., Vömel, H., Oltmans, S. J., and Rosenlof, K. H.: Transport into the northern hemisphere lowermost stratosphere revealed by in situ tracer measurements, J. Geophys. Res., 104, 26 565–26 580, 1999.
Scheeren, H. A., Fisher, H., Lelieveld, J., Hoor, P., Rudolph, J., Arnold, F., Bregman, B., Bruehl, C., Engel, A., van der Veen, C., and Brunner, D.: Reactive organic species in the northern extratropical lowermost stratosphere: Seasonal variability and implications for OH, J. Geophys. Res., 108(D24), 4805, doi:10.1029/2003JD003650, 2003.
Siegmund, P. C., van Velthoven, P. F. J., and Kerder, H.: Cross-tropopause transport in the extratropical northern winter hemisphere, diagnosed from high resolution ECMWF data, Q. J. R. Meteorol. Soc., 122, 1921–1941, 1996.
Sigmond, M., Meloen, J., and Siegmund, P. C.: Stratosphere-troposphere exchange in an extratropical cyclone, calculated with a Lagrangian method, Ann. Geophys., 18, 573–582, 2000.
Simmons, A. J., Untch, A., Jakob, C., Kallberg, P., and Unden, P.: Stratospheric water vapour and tropical tropopause temperatures in ECMWF analyses and multi-year simulations, Q. J. R. Meteorol Soc., 125, 353–386, 1999.
Stohl, A., Cooper, O. R., and James, P.: A cautionary note on the use of meteorological analysis fields for quantifying atmospheric mixing, J. Atmos. Sci., 61, 1446–1453, 2004.

Traub, M. and Lelieveld, J.: Cross-tropopause transport over the eastern Mediterranean, J. Geophys. Res., 108(D23), 4712, doi:10.1029/2003JD003754, 2003.

Vaughan, G. and Timmis, C.: Transport of near-tropopause air into the lower midlatitude stratosphere, Q. J. R. Meteorol. Soc., 124, 1559–1578, 1998.

Vömel, H., Rummukainen, M., Kivi, R., Karhu, J., Turunen, T., Kyrö, E., Rosen, J., Kjome, N., and Oltmans, S.: Dehydration and sedimentation of ice particles in the Arctic stratospheric vortex, Geophys. Res. Lett., 24, 795–798, 1997.

Wei, M.-Y.: A new formulation of the exchange of mass and trace constituents between the stratosphere and the troposphere, J. Atmos. Sci., 44, 3079–3086, 1987.

Wernli, H. and Bourqui, M.: A Lagrangian "1-year climatology" of (deep) cross-tropopause exchange in the extratropical Northern Hemisphere, J. Geophys. Res., 107(D2), 4021, doi:10.1029/2001JD000812, 2002.

Wirth, V. and Egger, J.: Diagnosing extratropical synoptic-scale stratosphere-troposphere exchange: A case study, Q. J. R. Meteorol. Soc., 125, 635–655, 1999.

Yushkov, V., Astakhov, V., and Merkulov, S.: Optical balloon hygrometer for upper-troposphere and stratosphere water vapor measurements, in: Optical Remote Sensing of the Atmosphere and Clouds, edited by: Wang, J., Wu, B., Ogawa, T., Z-h Guans, Proc. SPIE vol. 3501, pp. 439–445, 1998.

Yushkov, V., Merkulov, S., Astakhov, V., Pommereau, J. P., and Garnier, A.: A Lyman alpha hygrometer for long duration IR Montgolfier during the THESEO Lagrangian Experiment, Proc. 5th European Ozone Workshop, EC Air Pollution Report 73, 400–403, 2000.

Zierl, B. and Wirth, V.: The influence of radiation on tropopause behaviour and stratosphere-troposphere exchange in an upper tropospheric anticyclone, J. Geophys. Res., 102(D20), 23 883–23 894, 1997.

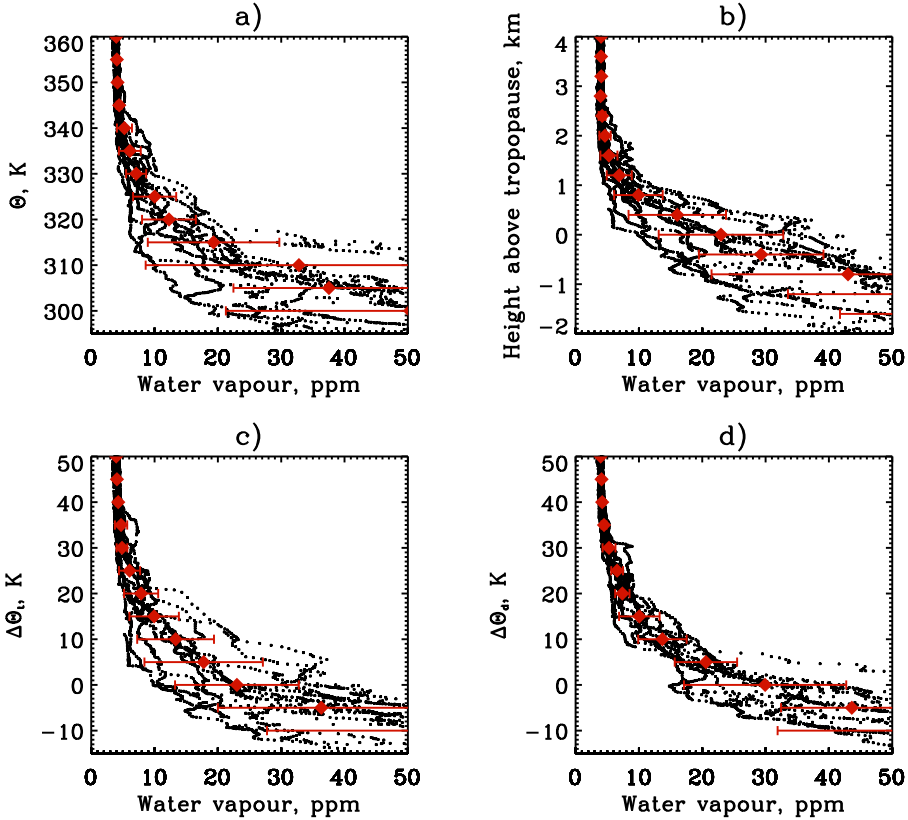

Fig. 1. WVMR as a function of **(a)** potential temperature, **(b)** height above the thermal tropopause, **(c)** $\Delta\theta$ above the thermal tropopause, **(d)** $\Delta\theta$ above the dynamical tropopause. WVMR averaged over all flights and one standard deviation are shown in red.

ACPD
6, 4727–4754, 2006

EGU

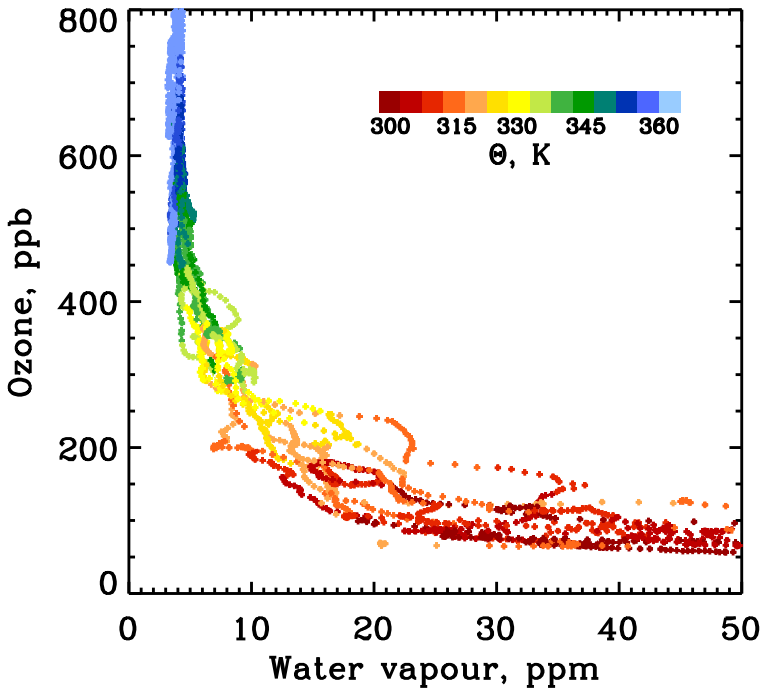

Fig. 2. Scatter plot of water vapour and ozone mixing ratios. The potential temperature is coded by colours.

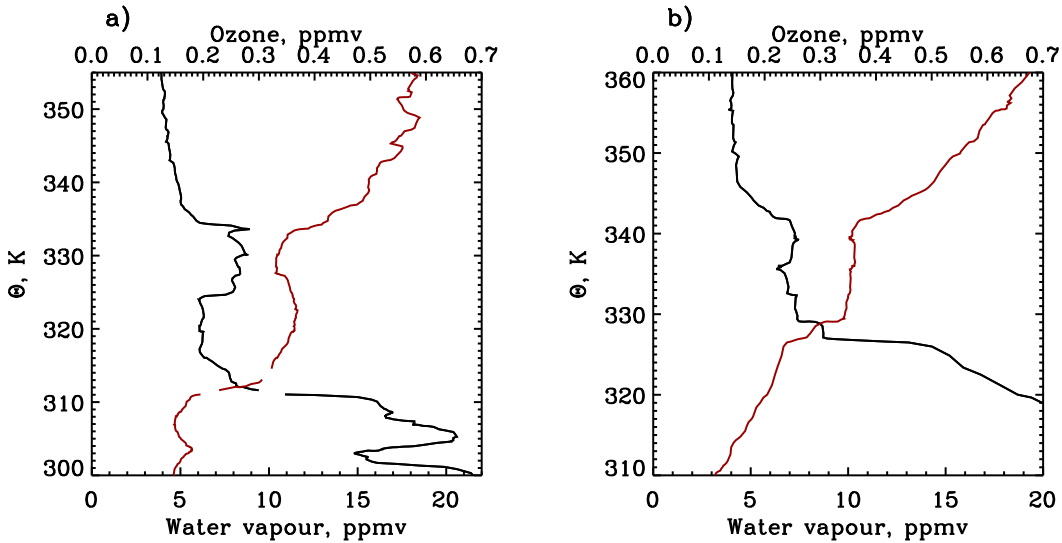

Fig. 3. Water vapour and ozone mixing ratios as a function of potential temperature on **(a)** 17 February 2004, 18:00 UTC, and **(b)** 24 February 2004, 18:00 UTC.

ACPD
6, 4727–4754, 2006

EGU

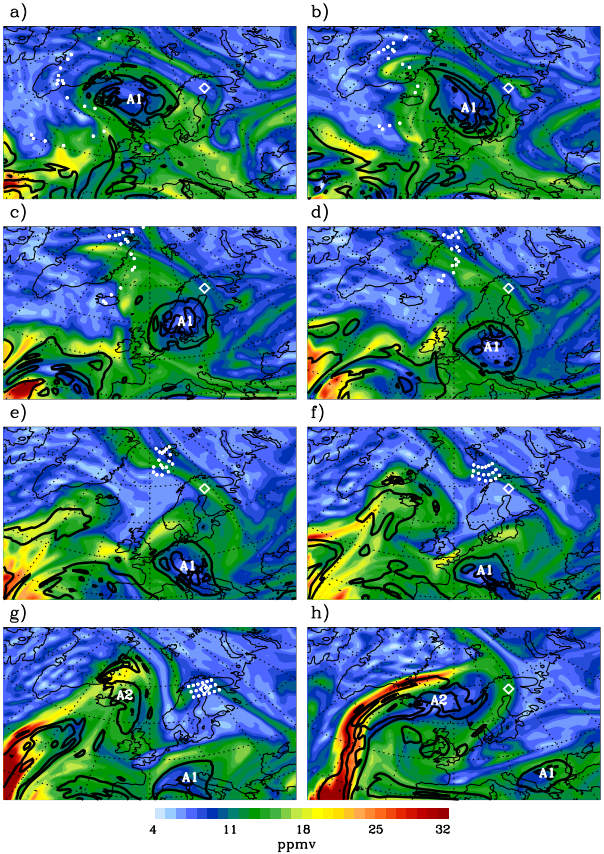

Fig. 4. ECMWF WVMR maps at the 330 K isentropic surface on **(a)** 14 February 2004, 18:00 UTC, **(b)** 15 February 2004, 06:00 UTC, **(c)** 15 February 2004, 18:00 UTC, **(d)** 16 February 2004, 06:00 UTC, **(e)** 16 February 2004, 18:00 UTC, **(f)** 17 February 2004, 06:00 UTC, **(g)** 17 February 2004, 18:00 UTC and **(h)** 18 February 2004, 18:00 UTC. Black thick lines mark 2 and 3.5 PVU contours of PV. White dots in (a–g) indicate the positions of the backward isentropic trajectories initiated on 17 February 2004, 18:00 UTC. The white diamond indicates the location of Sodankyla. A1 and A2 indicate the positions of the anticyclones discussed in the text.

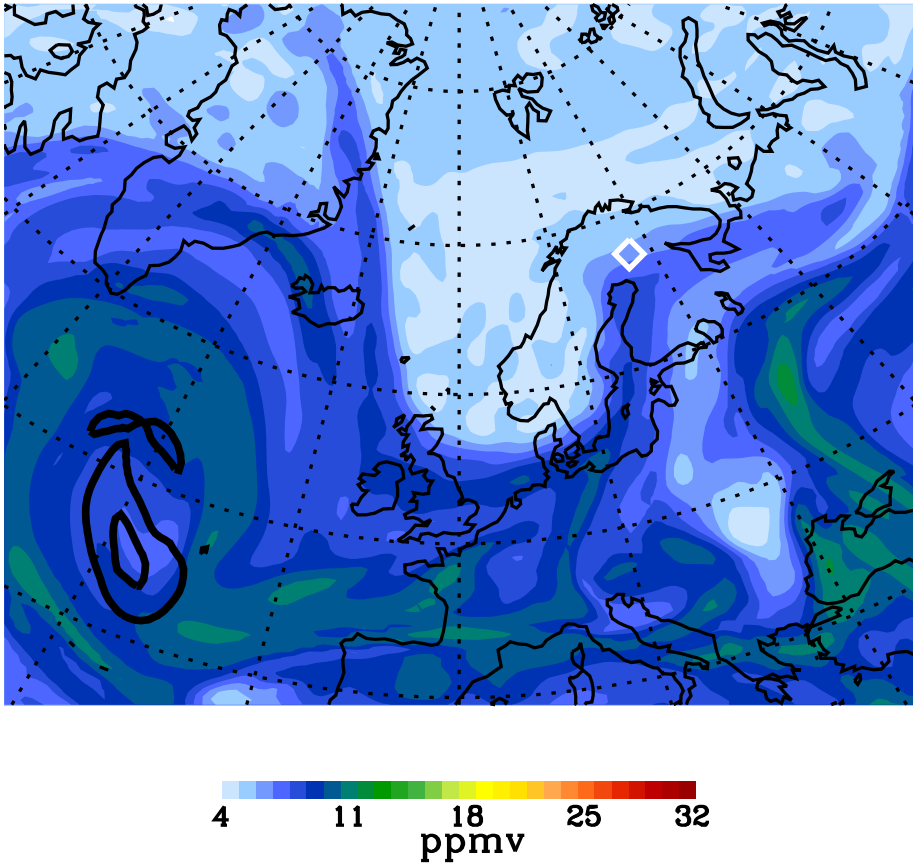

Fig. 5. ECMWF WVMR map at the 340 K isentropic surface on 24 February 2004, 18:00 UTC. Black thick lines mark 2 and 3.5 PVU contours of PV. The white diamond indicates the location of Sodankylä.

ACPD
6, 4727–4754, 2006

EGU

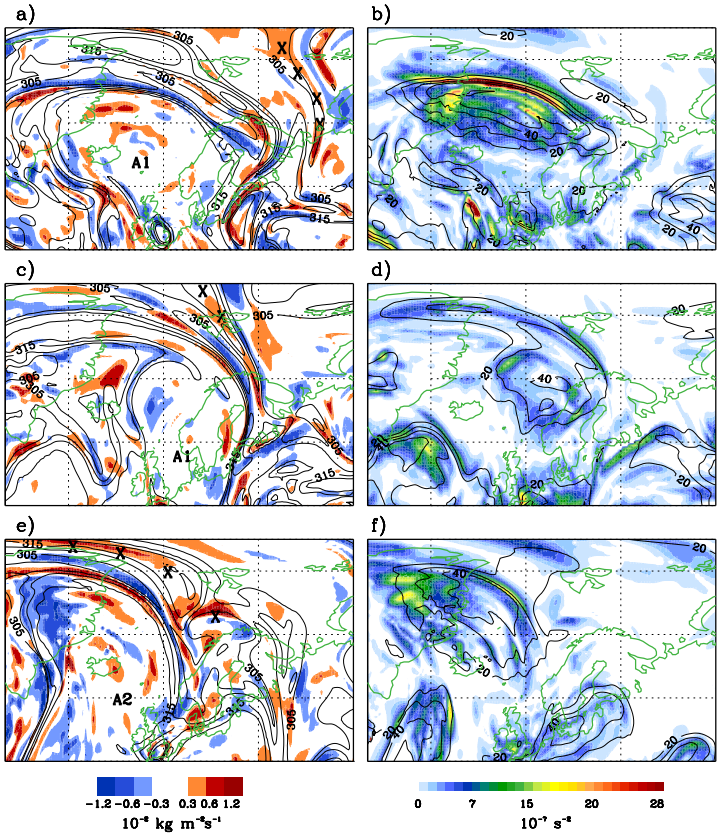

Fig. 6. (a, c, e) CTF across 3.5 PVU isosurface of PV and **(b, d, f)** CAT index on (a, b) 14 February 2004, 18:00 UTC, (c, d) 15 February 2004, 18:00 UTC, and (e, f) 17 February 2004, 12:00 UTC. Black solid lines are (a, c, e) potential temperature contours (K) and (b, d, f) wind speed contours (m/s). A1 and A2 indicate the positions of the anticyclones. The crosses indicate the positions of the filaments discussed in the text.

ACPD
6, 4727–4754, 2006

EGU

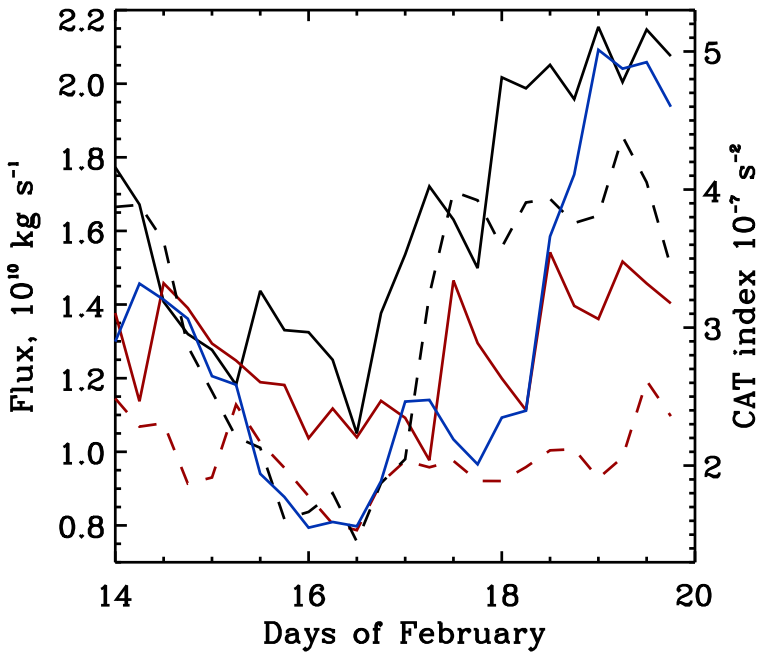

Fig. 7. Time series of CAT index and absolute values of downward and upward CTF averaged over the domain 310° W–60° E and 60° N–85° N. Solid lines are CTF calculated from analyses; dashed lines are those from forecasts. Downward CTF is black, upward CTF is red, CAT index is blue.

ACPD
6, 4727–4754, 2006

EGU